Energy & Environmental Science

PAPER

View Article Online
View Journal | View Issue

Cite this: *Energy Environ. Sci.*, 2018, **11**, 1779

Comprehensive control of voltage loss enables 11.7% efficient solid-state dye-sensitized solar cells†

Weiwei Zhang,[ab] Yongzhen Wu,*[a] Hee Won Bahng,[c] Yiming Cao,[b] Chenyi Yi,[b] Yasemin Saygili,[d] Jingshan Luo,[b] Yuhang Liu,[b] Ladislav Kavan,[be] Jacques-E. Moser,[c] Anders Hagfeldt,[d] He Tian,[a] Shaik Mohammed Zakeeruddin,*[b] Wei-Hong Zhu*[a] and Michael Grätzel*[b]

Received 4th March 2018,
Accepted 16th April 2018

DOI: 10.1039/c8ee00661j

rsc.li/ees

The relatively large voltage loss (V_{loss}) in excitonic type solar cells severely limits their power conversion efficiencies (PCEs). Here, we report a comprehensive control of V_{loss} through efficacious engineering of the sensitizer and redox mediator, making a breakthrough in the PCE of dye-sensitized solar cells (DSSCs). The targeted down-regulation of V_{loss} is successfully realized by three valid channels: (i) reducing the driving force of electron injection through dye molecular engineering, (ii) decreasing the dye regeneration overpotential through redox mediator engineering, and (iii) suppressing interfacial electron recombination. Significantly, the "trade-off" effect between the dye optical band gap and the open-circuit voltage (V_{OC}) is minimized to a great extent, achieving a distinct enhancement in photovoltaic performance (PCE > 11.5% with V_{OC} up to 1.1 V) for liquid junction cells. The solidification of the best-performing device leads to a PCE of 11.7%, which is so far the highest efficiency obtained for solid-state DSSCs. Our work inspires further development in highly efficient excitonic solar cells by comprehensive control of V_{loss}.

Broader context

Excitonic type solar cells, including dye-sensitized solar cells (DSSCs), perovskite solar cells (PSCs) and organic solar cells (OSCs), are potential alternatives for photovoltaic applications. To further advance their power conversion efficiencies (PCEs), it is crucial to reduce the so called voltage loss (V_{loss}) as much as possible. In DSSCs, the V_{loss} mainly takes place in the electron injection, dye regeneration and interfacial recombination processes, whereas the targeted decreasing of V_{loss} in all these aspects has been rarely reported. To address this issue, we herein demonstrate a comprehensive control of V_{loss}, achieving 11.7% efficiency for solid-state DSSCs. This work is a good example of radically improving the PCE through rationally reducing V_{loss}.

Introduction

Dye-sensitized solar cells (DSSCs)[1] have many advantages over traditional photovoltaic (PV) technologies, including their low fabrication cost, attractive aesthetics and benign environmental compatibilities.[2–5] However, their power conversion efficiency (PCE) hampers practical applications, especially for solid-state DSSCs which are believed to have practical advantages. Compared to PVs based on inorganic semiconductors or organic–inorganic hybrid perovskites, DSSCs are subjected to a relatively large voltage loss[6,7] ($V_{loss} = E_g - V_{OC}$, where E_g is the HOMO–LUMO separation of the sensitizer, and V_{OC} is the open-circuit voltage of the solar cells). The large V_{loss} is one of the most important origins of the limit of the PCE of DSSCs, which mainly arises from three aspects:[8–10] (i) the electron injection V_{loss} originating from an excess over-potential of electron transfer from the photoexcited

[a] *Key Laboratory for Advanced Materials and Institute of Fine Chemicals, Shanghai Key Laboratory of Functional Materials Chemistry, School of Chemistry and Molecular Engineering, East China University of Science and Technology, Shanghai 200237, China. E-mail: wu.yongzhen@ecust.edu.cn, whzhu@ecust.edu.cn*

[b] *Laboratory of Photonics and Interfaces, Institute of Chemical Sciences and Engineering, École Polytechnique Fédérale de Lausanne (EPFL), 1015 Lausanne, Switzerland. E-mail: shaik.zakeer@epfl.ch, michael.graetzel@epfl.ch*

[c] *Photochemical Dynamics Group, Institute of Chemical Sciences and Engineering, École Polytechnique Fédérale de Lausanne (EPFL), 1015 Lausanne, Switzerland*

[d] *Laboratory of Photomolecular Science, Institute of Chemical Sciences and Engineering, École Polytechnique Fédérale de Lausanne (EPFL), 1015 Lausanne, Switzerland*

[e] *J. Heyrovsky Institute of Physical Chemistry, 18223 Prague, Czech Republic*

† Electronic supplementary information (ESI) available: Synthesis, characterization, and additional photovoltaic data. See DOI: 10.1039/c8ee00661j

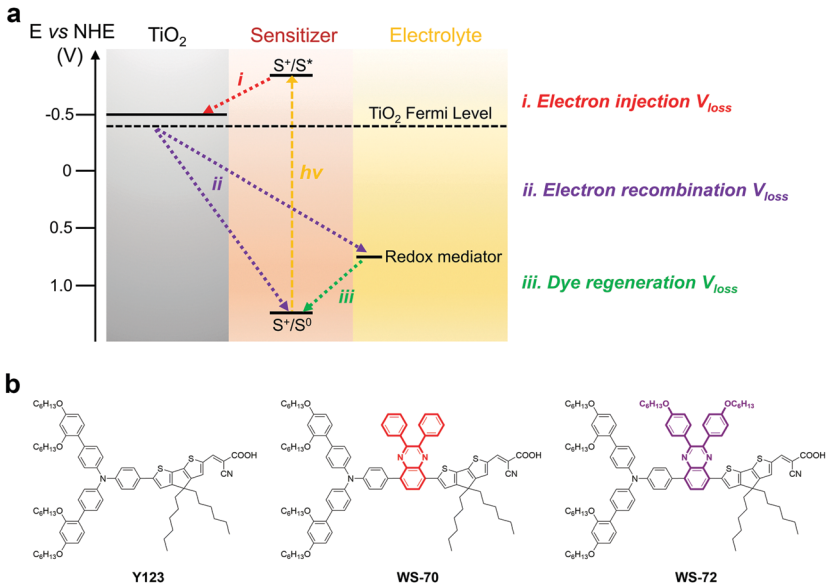

Fig. 1 (a) Schematic representation of three voltage losses in DSSCs. (b) Molecular structures of dyes **Y123**, **WS-70** and **WS-72**.

dye to titanium dioxide, (ii) the electron recombination V_{loss} caused by the recapture of injected electrons by the oxidized dye or redox shuttle, and (iii) the dye regeneration V_{loss} arising from an excess driving force for dye recovery by redox mediators (Fig. 1a).

To decrease the V_{loss} and improve the PCE for DSSCs, the over-potentials that provide the driving force for the electron injection and dye regeneration processes should be effectively minimized, and the electron recombination at the TiO_2/dye/electrolyte interfaces should be efficiently suppressed. Previous optimizations of DSSCs were mainly based on the development of new materials, including n-type metal oxides, photosensitizers, redox shuttles and counter electrode materials.[11–19] The improvements of PCE were usually associated with a decrease in V_{loss} to some extent.[20–29] However, a targeted down-regulation of V_{loss}, which simultaneously reduces the V_{loss} involved in electron injection, dye regeneration and interfacial recombination processes, is scarcely reported.

Here, we report a comprehensive control of V_{loss} in DSSCs through judicious molecular engineering of the sensitizer and the redox mediator. By introducing a quinoxaline based auxiliary acceptor into the molecular structure of the well-known dye **Y123** between the donor and π-bridge (4,4-dihexyl-4*H*-cyclopenta[2,1-*b*:3,4-*b*′]dithiophene, CPDT), we develop two novel dyes **WS-70** and **WS-72** (Fig. 1b) with targeted modulation of the lowest unoccupied molecular orbital (LUMO) levels, affording a decrease in V_{loss} for electron injection from the excited sensitizer into the conduction band of the metal oxide. The associated downward shift of their highest occupied molecular orbital (HOMO) levels is efficiently converted to a V_{OC} enhancement by the control of dye regeneration V_{loss}. Furthermore, a significant decrease of the electron recombination V_{loss} is achieved through elaborate design of the quinoxaline based auxiliary acceptor, which greatly suppresses the interception of injected electrons by oxidized dyes and redox mediators as demonstrated in laser flash photolysis and electrochemical impedance spectroscopy experiments. As a consequence, the comprehensive control of V_{loss} results in a remarkable minimization of the "trade-off" effect between the dye optical band gap and the V_{OC} value. Simultaneously, a distinct enhancement in photovoltaic performance is realized, along with a high V_{OC} of 1.1 V for liquid junction cells, which is comparable to that of the best performing perovskite solar cell. The solidification of the electrolyte for the champion device leads to a PCE of 11.7%, which is so far the highest efficiency for solid-state DSSCs.

Results and discussion

Targeted reduction in the electron injection V_{loss} through dye molecular engineering

Donor–π–acceptor (D–π–A) featuring organic sensitizers have been widely explored for application in DSSCs.[30–34] Dye **Y123** is one of the most popular pure-organic photosensitizers, which has the merits of a simple molecular structure, high optical absorption coefficients and excellent photovoltaic performance in both liquid and solid state DSSCs.[30,34] However, dye **Y123** has a high lying LUMO energy level (∼−1.0 V *vs.* normal hydrogen electrode (NHE)) due to the electron-rich nature of the triphenylamine based donor and the CPDT based π-spacer, which leads to a considerable electron injection V_{loss}. Previously, our group proposed the concept of a D–A–π–A motif by introducing an auxiliary acceptor between the donor and π-spacer of the D–π–A sensitizer. The auxiliary acceptor was proved to be able to downwards shift the LUMO level and broaden the absorption spectrum.[35,36] Here, to decrease the electron injection V_{loss} for dye **Y123**, we purposefully incorporate auxiliary acceptors (based on quinoxaline) into the skeleton of dye **Y123** to afford two novel dyes **WS-70** and **WS-72** (Fig. 1b, for synthesis and characterization see ESI†).

Fig. 2a shows the ultraviolet-visible (UV-vis) absorption spectra of dyes **Y123**, **WS-70** and **WS-72** measured in

dichloromethane solution. The corresponding data are summarized in Table S1 (ESI†). **Y123** shows the intramolecular charge transfer (ICT) peak at 541 nm with a molar extinction coefficient (ε) of 5.24 × 10^4 M^{-1} cm^{-1}. When introducing the quinoxaline based auxiliary acceptor into the **Y123 dye** framework, **WS-70** and **WS-72** display a similar ICT band with peaks at 542 and 545 nm, respectively. Meanwhile, the molar extinction coefficients for **WS-70** and **WS-72** increase to 6.23 × 10^4 and 5.88 × 10^4 M^{-1} cm^{-1} respectively for the ICT peak, exceeding that of **Y123**. Upon adsorption onto 2 μm thick TiO_2 films (Fig. 2b), all three dyes show a blue-shift in absorption due to the deprotonation of carboxylic acid. We note that dyes **WS-70** and **WS-72** exhibit a smaller degree of blue shift with respect to **Y123** (28 and 31 nm *versus* 55 nm) due to the incorporation of auxiliary acceptors.

To investigate the energy level variation resulting from the dye molecular engineering, cyclic voltammetry measurements were performed on dyes adsorbed on TiO_2 films using an acetonitrile electrolyte solution (Fig. S1, ESI†). The corresponding redox potentials of **Y123**, **WS-70** and **WS-72** are 1.07, 1.12 and 1.15 V (*versus* NHE), respectively, which are assigned to their HOMO levels. The zero–zero transition energies ($E_{0\text{-}0}$) were determined from the absorption thresholds of dye-adsorbed TiO_2 films and shrunken energy gaps were obtained for **WS-70** and **WS-72** with respect to **Y123** (Fig. 2c and Table 1). It is noteworthy that LUMO values evaluated from the HOMO levels and $E_{0\text{-}0}$ exhibit an obvious downward shift from **Y123** (−0.94 V) to **WS-70** (−0.85 V) to **WS-72** (−0.82 V), resulting in a remarkably minimized energy difference between the dye LUMO levels and the TiO_2 conduction band (−0.5 V *vs.* NHE).

To evaluate the influence of the downwards shift in dye LUMO levels, *i.e.* the decrease of electron injection V_{loss}, on the electron injection yield, we compared the photovoltaic performance

Table 1 Energy levels of dyes **Y123**, **WS-70** and **WS-72**, and their photovoltaic performances based on the $[Co(bpy)_2]^{3+/2+}$ redox mediator

Dye	HOMO[a] (V)	$E_{0\text{-}0}$[b] (eV)	LUMO[c] (V)	J_{SC} (Cal)[d] (mA cm^{-2})	J_{SC}[e] (mA cm^{-2})	V_{OC}[e] (V)	FF	η[e] (%)
Y123	1.07	2.01	−0.94	13.9	14.1	0.87	0.74	9.2
WS-70	1.12	1.97	−0.85	14.1	14.1	0.90	0.76	9.7
WS-72	1.15	1.97	−0.82	14.2	14.2	0.93	0.77	10.3

[a] HOMO values were obtained from cyclic voltammetry of dyes adsorbed on TiO_2 in the acetonitrile electrolyte solution. [b] $E_{0\text{-}0}$ was determined from absorption thresholds of dye adsorbed onto 2 μm thick transparent TiO_2 films. [c] LUMO values were calculated according to LUMO = HOMO − $E_{0\text{-}0}$. [d] Calculated J_{SC} from the IPCE spectrum. [e] Measured under AM 1.5 G illumination (100 mW cm^{-2}).

of three dyes in DSSCs with $[Co(bpy)_3]^{3+/2+}$ mediated liquid electrolyte. Fig. 2d shows their monochromatic incident photon-to-electron conversion efficiency (IPCE) spectra. The IPCE heights for **WS-70** and **WS-72** are comparable to or even higher than that of **Y123** in the region of 350–750 nm with the highest value around 80%. Generally, by taking the absorption and reflection of the conductive glass into account, an IPCE plateau of DSSCs between 80 and 90% means near unity internal quantum efficiency for photoinduced charge carrier generation. This includes η_{inj} (electron injection efficiency), η_{reg} (dye regeneration efficiency) and η_{col} (charge collection efficiency). We found that the **WS-72** dye-based DSSCs showed even slightly higher IPCE than those of dye **WS-70** and **Y123** (Fig. 2d), although the LUMO energy level of the former is the lowest. This means that reducing the driving force had negligible influence on the electron injection efficiency (Fig. S8–S10, ESI†). Therefore, the targeted reduction of electron injection V_{loss} through molecular engineering is successful.

Fig. 2e shows the photocurrent density–voltage (J–V) curves under AM 1.5 G illumination (100 mW cm^{-2} at 298 K) and the

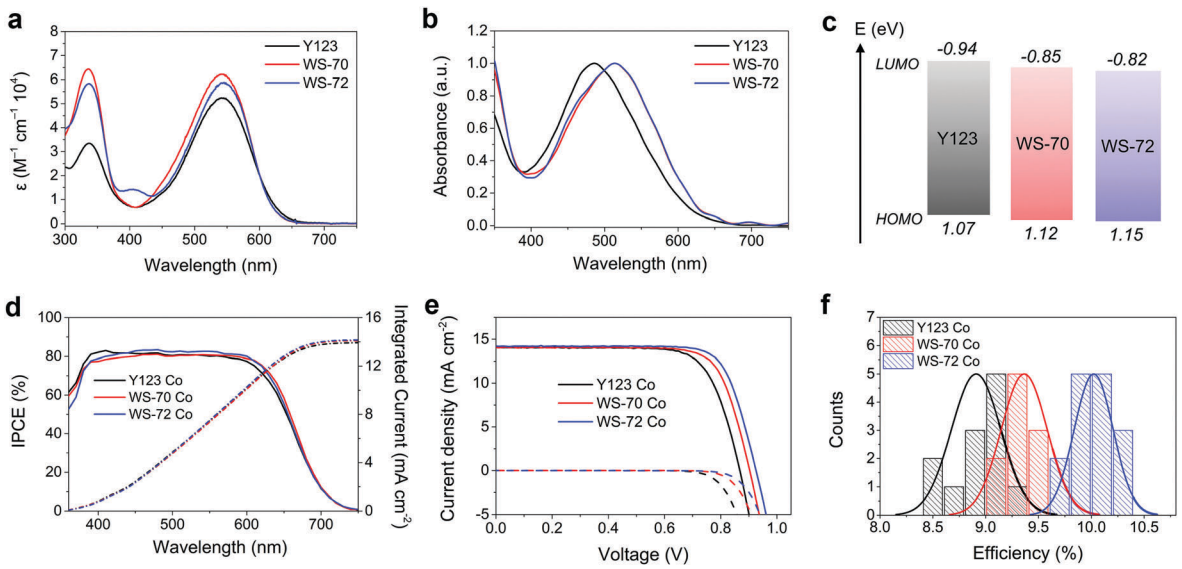

Fig. 2 (a and b) UV-vis spectra of dyes measured in dichloromethane and on 2 μm thick transparent TiO_2 films. (c) Schematic illustration of the LUMO (above the colored bar) and HOMO (under the colored bar) energy levels of the sensitizers. (d) IPCE spectra for DSSCs based on dyes **Y123**, **WS-70** and **WS-72** with the $[Co(bpy)_3]^{3+/2+}$ redox shuttle. (e) J–V curves of the corresponding DSSCs measured under AM 1.5 G illumination (100 mW cm^{-2}, solid lines) and in dark (dashed lines). (f) Histogram plots of solar cell efficiencies (12 individual devices for **Y123** and **WS-70**, 15 individual devices for the best performing sensitizer **WS-72**).

corresponding photovoltaic parameters are collected in Table 1. More detailed measurements under various light intensities are carried out and the results are shown in Fig. S2 and Table S2 (ESI†). In agreement with the IPCE results, all three dyes generated very similar J_{SC} values, while dyes **WS-70** and **WS-72** showed prominently improved V_{OC} performance with respect to **Y123**. The PCE gradually increased from 9.2% (**Y123**) to 9.7% (**WS-70**) and 10.3% (**WS-72**). The statistical efficiencies of DSSCs based on the three sensitizers are presented in Fig. 2f, which reveals good reproducibility of the fabricated cell devices.

Targeted reduction in the dye regeneration V_{loss} through redox mediator engineering

We note that the strategy of incorporating an auxiliary acceptor for decreasing electron injection V_{loss} also induces a downwards shift in the HOMO energy levels (Fig. 2c). Actually, this is a very common and thorny problem for sensitizer design subject to synchronous shifts in both HOMO and LUMO levels, which could cause additional V_{loss} in the electron injection or the dye regeneration process.[24,37] Here, to adapt to the lowering of the HOMO level in the new dyes and further reduce the V_{loss} in the dye regeneration process, we manipulated the redox shuttle from the $[Co(bpy)_3]^{3+/2+}$ (0.56 V *vs.* NHE) to $[Cu(tmby)_2]^{2+/+}$ (0.87 V *vs.* NHE), which possesses a more positive redox potential (Fig. 3a). This modification decreases the energy difference between the Nernst potential of the redox shuttle and the HOMO levels of the sensitizers. Except for the downward shifted redox potential, the $[Cu(tmby)_2]^{2+/+}$ based redox mediators have higher diffusion coefficients and a faster dye regeneration rate than that of $[Co(bpy)_3]^{3+/2+}$.[31] Notably, when employing a $[Cu(tmby)_2]^{2+/+}$ redox mediator, all three dyes displayed greatly enhanced overall photovoltaic performances (Fig. 3b, c and Table 2, and Fig. S3, S4 and Table S3, ESI†). The V_{OC} values are universally increased by 160–170 mV with respect to that of $[Co(bpy)_3]^{3+/2+}$ based devices. Strikingly, the new dye **WS-72** cell exhibits a greatly improved V_{OC} value of 1.1 V, which is above that of previously reported high-efficiency DSSCs using cobalt-complexes as mediators and matches the V_{OC} of highly performing perovskite solar cells.[11,12,17,38] Compared to a few previously reported high V_{OC} results that were realized by using dyes with large absorption energies,[29,39] this "trade-off" effect between the dye optical band gap and the V_{OC} value is largely minimized here. The total V_{loss} derived from the IPCE onset and the V_{OC} performance for **WS-72** based DSSCs was successfully reduced to 600 mV. We compared our results with a series of highly performing DSSCs that were reported in the literature (Table S4, ESI†), it can be clearly seen that the V_{loss} of 0.6 V in the present work is the smallest one when compared to other high efficiency DSSCs. Consequently, an impressive efficiency of 11.6% was achieved by the **WS-72** cell, with J_{SC} = 13.3 mA cm^{-2} and FF = 0.78. A slight decrease in the J_{SC} was observed for $[Cu(tmby)_2]^{2+/+}$ based devices with respect to that of $[Co(bpy)_3]^{3+/2+}$. This can be ascribed to the competitive optical absorption of the copper redox mediator and the quenching of the dye's excited state by $[Cu(tmby)_2]^{2+}$,[26,31] as revealed in the IPCE action spectra (Fig. 3d). Thus, through the reduction of the electron injection V_{loss}, and redox shuttle engineering which attenuated the dye regeneration V_{loss}, we attained a substantial improvement in V_{OC} for the new dye **WS-72**, along with an enhancement of the PCE from 10.3% to 11.6%.

Targeted reduction of the recombination V_{loss} by suppressing the recapture of injected electrons

Except for the electron injection and dye regeneration related V_{loss}, the electron recombination occurring at the TiO_2/dye/electrolyte interfaces can also cause a V_{loss} thus limiting the PCE. It is well known that electrons injected into TiO_2 could suffer from recombination by two electron transfer pathways,

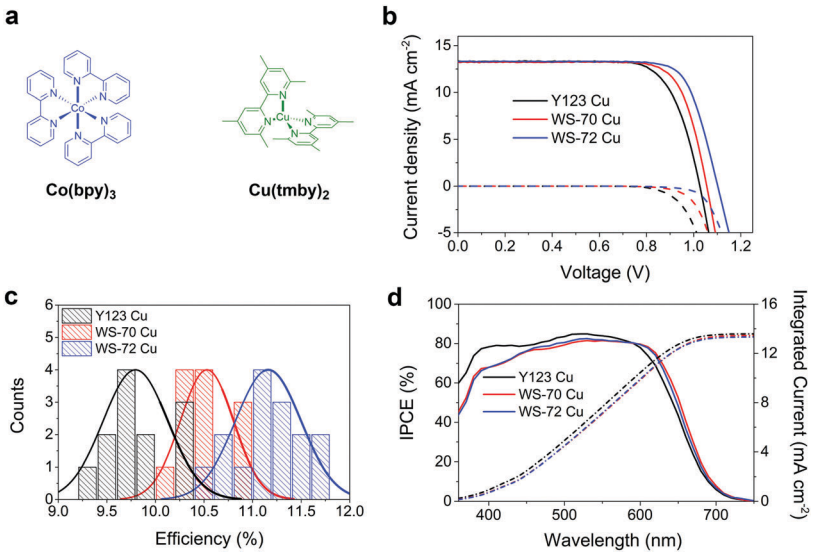

Fig. 3 (a) Chemical structures of the $[Co(bpy)_3]^{3+/2+}$ and $[Cu(tmby)_2]^{2+/+}$ redox shuttles. (b) *J*–*V* curves for DSSCs fabricated with dyes **Y123**, **WS-70** and **WS-72** employing the $[Cu(tmby)_2]^{2+/+}$ redox shuttle measured under AM 1.5 G illumination (100 mW cm^{-2}, solid lines) and in dark (dashed lines). (c) Histogram plots of solar cell efficiencies (12 individual devices for **Y123** and **WS-70**, 15 individual devices for the best performing sensitizer **WS-72**). (d) IPCE spectra for DSSCs based on the $[Cu(tmby)_2]^{2+/+}$ redox shuttle.

Table 2 Photovoltaic performance of DSSCs fabricated with dyes **Y123**, **WS-70** and **WS-72** employing the $[Cu(tmby)_2]^{2+/+}$ redox mediator measured under AM 1.5 G illumination (100 mW cm^{-2})

Dyes	J_{SC} (Cal) (mA cm^{-2})	J_{SC} (mA cm^{-2})	V_{OC} (V)	FF	η (%)
Y123	13.6	13.6	1.03	0.74	10.3
WS-70	13.5	13.2	1.06	0.77	11.0
WS-72	13.3	13.3	1.10	0.78	11.6

J_{SC} (Cal) values were calculated from the IPCE spectra.

(i) to the oxidized form of the sensitizer, (ii) to the redox shuttle in the electrolyte[8] (Fig. 1). Fig. 4a shows the results of laser flash photolysis experiments for three dyes (**Y123**, **WS-70** and **WS-72**), which were performed with dye adsorbed on TiO_2 films in the presence of inert electrolytes (without redox shuttles). In this case, after dye excitation and electron injection, the oxidized dye returns to the initial state by recapturing the electrons from the TiO_2. Thereby, the time constants (τ_{rec}) deduced from the dye transient absorption decay reflect the recombination rate of electrons in TiO_2 with an oxidized sensitizer. As summarized in Table S5 (ESI†), **Y123** displayed a τ_{rec} of 4.5 ms. By comparison, **WS-70** and **WS-72** exhibited almost two (9.5 ms) and three times (13 ms) longer τ_{rec}, respectively, indicative of a much slower back electron transfer rate. Apparently, incorporation of the quinoxaline based auxiliary acceptor can effectively suppress the recapture of injected electrons by the oxidized sensitizer, attenuating the V_{loss} of this recombination channel.

To evaluate the recombination kinetics of injected electrons with the redox shuttles, we further performed electrochemical impedance spectroscopy (EIS) measurements on the DSSCs fabricated with dyes **Y123**, **WS-70** and **WS-72**, employing both $[Co(bpy)_3]^{3+/2+}$ and $[Cu(tmby)_2]^{2+/+}$ based electrolytes.[40] Fig. 4b and c plot the charge transfer resistance (R_{CT}) at the TiO_2/dye/electrolyte interfaces against different bias potentials. We note that the interfacial recombination process is closely related to the electron density in TiO_2. As the Nernst potential of $[Cu(tmby)_2]^{2+/+}$ is lower than that of $[Co(bpy)_3]^{3+/2+}$, the electron density will be lower for the former when the bias potential is the same. Therefore, the R_{CT} of $[Cu(tmby)_2]^{2+/+}$ based DSSCs were larger than that of $[Co(bpy)_3]^{3+/2+}$ at a low bias condition (Fig. 4b and c). However, when the bias potential was near their V_{OC}, the R_{CT} of $[Cu(tmby)_2]^{2+/+}$ based DSSCs became slightly smaller than that of $[Co(bpy)_3]^{3+/2+}$. For both electrolytes, the R_{CT} was found to remarkably increase with an order of **Y123** < **WS-70** < **WS-72** for both redox systems, suggesting the suppressed recapture of the injected electrons by the oxidized redox mediator. We believe that the quinoxaline unit with two phenyl groups in **WS-70** is favorable for the formation of a compact dye assembly layer on the surface of TiO_2,[41] preventing the contact of oxidized redox species ($[Co(bpy)_3]^{3+}$ and $[Cu(tmby)_2]^{2+}$) with the injected electrons. By further modifying the quinoxaline based auxiliary acceptor with two decorated hexyloxy chains on the phenyl, **WS-72** exhibits an even stronger capability to block the recombination process (R_{CT} being two times larger than for **Y123**). Overall, we have distinctly reduced the recombination V_{loss} by suppressing the recapture of injected electrons by both the oxidized sensitizer and the redox mediators through interfacial dye assembly engineering.

The slower charge recombination contributes to a longer electron lifetime and the accumulation of electrons in TiO_2. Upon charge dynamics characterization by transient photocurrent and photovoltage decay measurements (as shown in Fig. S5, ESI†), it can be observed that the electron lifetime is greatly prolonged from **Y123** to **WS-70** to **WS-72**, not only for the $[Co(bpy)_3]^{3+/2+}$ but also the $[Cu(tmby)_2]^{2+/+}$ based redox electrolytes. At a given V_{OC}, the electron lifetimes for **WS-70** and **WS-72** sensitized cells are nearly three and six times longer than that of **Y123**, respectively. The long lifetime resulting from low charge recombination greatly contributes to V_{OC} enhancement for **WS-72** based devices (see note in Fig. S5, ESI†).

Highly performing solid-state DSSCs

Thanks to the unique properties of the $[Cu(tmby)_2]^{2+/+}$ redox mediator that can be fabricated as a solid-state hole transport material (HTM),[16,30] we slowly evaporated the electrolyte solvent to produce solid-state DSSCs with the best performing dye **WS-72**. Significantly, we achieved an outstanding PCE of 11.7% (J_{SC} = 13.8 mA cm^{-2}, V_{OC} =1.07 V and FF = 0.79), exhibiting a small increase in J_{SC} and a slight decrease in V_{OC} as compared to the liquid-junction cell device (Fig. 5a and Table 3). To the best of our knowledge, this is the highest efficiency ever reported for solid-state DSSCs. The photocurrent dynamics as a function of various light intensities show that J_{SC} depends linearly on the light intensity, suggesting no limitation of the mass transport of the solid state

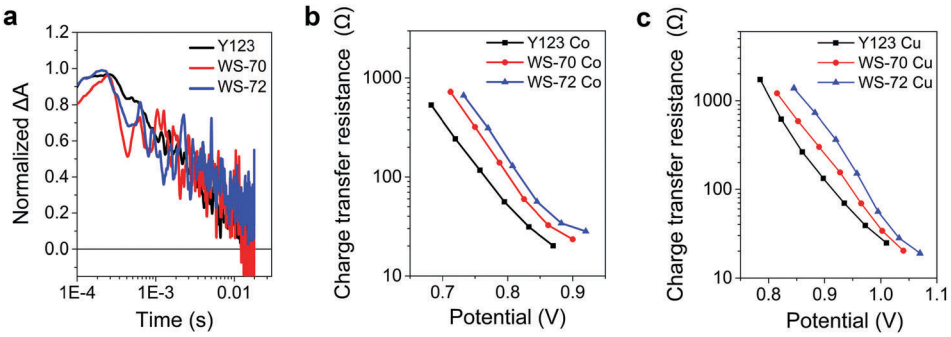

Fig. 4 (a) Flash photolysis measurements of dyes **Y123**, **WS-70** and **WS-72** adsorbed on mesoporous TiO_2 films with an inert electrolyte. Excitation wavelength at 525 nm, probe wavelength at 580 nm. (b and c) Charge transfer resistance at the TiO_2/dye/electrolyte interfaces for devices fabricated with dyes **Y123**, **WS-70** and **WS-72** employing $[Co(bpy)_3]^{3+/2+}$ (b) and $[Cu(tmby)_2]^{2+/+}$ (c) based electrolytes.

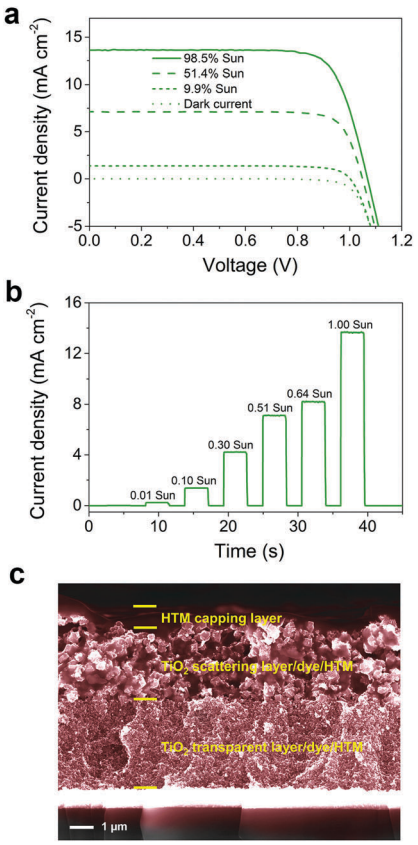

Fig. 5 (a) J–V curves for solid-state DSSCs fabricated with dye **WS-72** and $[Cu(tmby)_2]^{2+/+}$ based HTM under various light intensities. (b) Dependence of the photocurrent transient dynamics for solid-state DSSCs under various light intensities. (c) Cross sectional SEM of the solid-state DSSCs after removal of the PEDOT-coated FTO counter electrode.

Table 3 Photovoltaic performance of solid-state DSSCs fabricated with **WS-72** dye and $[Cu(tmby)_2]^{2+/+}$ based HTM measured under various light intensities

Dyes	P_{in} (mW cm^{-2})	J_{SC} (mA cm^{-2})	V_{OC} (V)	FF	η (%)
WS-72	100	13.8	1.07	0.79	11.7
	50	7.2	1.05	0.79	11.6
	10	1.4	0.99	0.77	10.3

redox mediators[42] (Fig. 5b). Moreover, the shelf lifetime of the best performing solid-state DSSCs was evaluated at room temperature (Fig. S6, ESI†). The device can retain 96% of its peak efficiency after 1000 h, indicating a promising stability of the optimized DSSCs system. A cross-sectional scanning electron microscopy (SEM, Fig. 5c) image shows the structure of the solid-state cell device (without the counter electrode). Energy dispersive X-ray spectroscopy analysis (Fig. S7, ESI†) shows the homogeneous infiltration of the copper based redox mediator from top to bottom in the mesoscopic TiO_2 films.

Conclusions

We have demonstrated a comprehensive control of the V_{loss} in DSSCs from the electron injection, dye regeneration and electron recombination processes by modulating the energy levels of the sensitizers and redox mediators, as well as the dye assembly on the TiO_2 surface. The significantly decreased V_{loss} brings forth a greatly improved V_{OC} performance with negligible sacrifice in J_{SC} when compared to the initial benchmark. As a result, the optimal dye **WS-72** employing a $[Cu(tmby)_2]^{2+/+}$ liquid-junction redox electrolyte generates a notable V_{OC} of 1.1 V along with an excellent PCE of 11.6% under AM 1.5 G illumination; a 26% improvement over that of reference dye **Y123**. The outstanding V_{OC} is comparable to that of a high performing perovskite solar cell. Compared to a few previously reported high V_{OC} values that were realized by using dyes with large absorption energies, the "trade-off" effect between the dye optical band gap and the V_{OC} value is largely minimized here. Moreover, the solidification of the liquid-junction devices leads to an even higher PCE of 11.7% (J_{SC} = 13.8 mA cm^{-2}, V_{OC} = 1.07 V and FF = 0.79). To the best of our knowledge, this represents the highest PCE for solid-state DSSCs so far. Our work is a good example of radically improving the PCE of DSSCs through comprehensive control of V_{loss}. Future work will focus on more elaborate optimization enhancing the long-wavelength-response of organic sensitizers to further boost their photovoltaic performance.

Experimental section

Materials

Toluene (Sigma-Aldrich), ethanol (Fluka), acetonitrile (ABCR), LiTFSI (TCI) and TBP (TCI) were used as received, unless stated otherwise. $[Co(bpy)_3]^{3+/2+}$ and $[Cu(tmby)_2]^{2+/+}$ redox shuttles and dye **Y123** were prepared in the same manner reported previously.[26,34,37] Starting materials 4,4-dihexyl-4*H*-cyclopenta[2,1-*b*:3,4-*b*′]dithiophene (**1**), 5,8-dibromo-2,3-diphenyl-4*a*,8*a*-dihydroquinoxaline (**2**), 5,8-dibromo-2,3-bis(4-(hexyloxy)phenyl)-2,3-dihydroquinoxaline (**5**), *N*-(2′,4′-bis(hexyloxy)-[1,1′-biphenyl]-4-yl)-2′,4′-bis(hexyloxy)-*N*-(4-(4,4,5,5-tetramethyl-1,3-dioxolan-2-yl)phenyl)-[1,1′-biphenyl]-4-amine (**8**) were synthesized according to the corresponding literature methods.[34,41,43] Tetrahydrofuran was dried by sodium under an argon atmosphere before use. 4,4-Dioctyl-4*H*-cyclopenta[2,1-*b*:3,4-*b*′]-dithiophene (**6**) were purchased from Derthon Co Ltd. Trimethylborate was purchased from Adamas Reagent Co Ltd. All other solvents and chemicals were purchased from Acros, Aldrich and used as received without further purification.

Devices fabrication

The fabrication of DSSCs followed the previous literature.[37] The procedures for preparing cell devices with $[Co(bpy)_3]^{3+/2+}$ and $[Cu(tmby)_2]^{2+/+}$ were similar except for the electrolyte composition and counter electrode (graphene nanoplatelets for $[Co(bpy)_3]^{3+/2+}$ and PEDOT for $[Cu(tmby)_2]^{2+/+}$). For photoanodes, FTO glasses (FTO, Solar 4 mm thickness, 10 ohms sq^{-1}, Nippon Sheet Glass) were first cleaned with a detergent solution (Deconex) in an ultrasonic bath (15 min), followed by water (15 min), acetone (15 min) and ethanol (15 min). This initial step was then followed by a UV/O_3 treatment (20 min). Afterwards, the substrates were immersed into a 53 mM $TiCl_4$ solution and kept at 70 °C in an oven for

30 minutes to form a compact TiO_2 blocking layer. The screen-printing transparent paste was composed of ~30 nm diameter anatase particles (30 NRD), and a scattering layer (400 nm diameter, Catalysts & Chemicals Ind. Co. Ltd (CCIC), HPW-400) was deposited on the top of transparent layer. The electrodes coated with the 8 μm TiO_2 pastes (4 μm transparent layer and 4 μm scattering layer) were sintered on hot plate. Afterwards, the TiO_2 electrodes were immersed into a 0.1 mM solution of **Y123**, **WS-70**, **WS-72** with 0.5 mM 3α,7α-dihydroxy-5β-cholic acid (chenodeoxycholic acid) in toluene/ethanol mixture (2/8 volume/volume) and kept for 16 h at room temperature. The dye sensitized electrodes were rinsed by acetonitrile and dried with nitrogen flow. For the counter electrodes of the $[Co(bpy)_3]^{3+/2+}$ system, the graphene nanoplatelets were prepared by drop casting of the suspension (2 mg mL^{-1} in acetone) on predrilled FTO (TEC 7, Pilkington) then heated to 450 °C for 2 min. For the $[Cu(tmby)_2]^{2+/+}$ system, the PEDOT films were prepared by electrochemical deposition on predrilled FTO glass. The working electrodes and counter electrodes were assembled in a dry box with 15 μm of Surlyn (DuPont). The electrolyte was injected into the device through a predrilled hole in the counter electrode under vacuum. The cobalt based electrolyte consists of 0.25 M $[Co(bpy)_3]$ $[B(CN)_4]_2$ and 0.06 M $[Co(bpy)_3]$ $[B(CN)_4]_3$ complexes with 0.1 M LiTFSI and 0.5 M 4-*tert*-butylpyridine in acetonitrile. The copper based electrolyte consists of 0.2 M $[Cu(tmby)_2]$ (TFSI) and 0.06 M $[Cu(tmby)_2]$ $(TFSI)_2$ complexes with 0.1 M LiTFSI and 0.6 M 4-*tert*-butylpyridine in acetonitrile. For solid state devices, the electrolyte solvent was evaporated in a dry box by keeping the holes on the counter electrode unsealed for a period of more than one week. Since acetonitrile solvent has a low boiling point of 81.6 °C and a high volatility, most of the solvent was removed during this process. To further confirm the absence of residual solvent in the cells, we kept the above evaporated devices in a high vacuum chamber connected to a vacuum pump for one hour, and measured the photovoltaic performance of the device before and after the vacuum treatment. The metrics remained unchanged upon vacuum treatment, indicating negligible residual solvent in the cells. A black mask (0.158 cm^2) was used in the subsequent photovoltaic studies to ensure an accurate measure of the area of incident light.

J–V characterization

The current density–voltage (*J–V*) characteristics were measured under a 450 W xenon light source (Oriel, USA). A Keithley model 2400 digital source meter (Keithley, USA) was used to apply an external potential bias to the devices and measure the resulting current. The Oriel was equipped with a SchottK113 Tempax sunlight filter (Praezisions Glas & OptikGmbH) to match the emission spectrum of the lamp to the AM 1.5 G standard. The light intensity was determined using a calibrated Si reference diode equipped with an infrared cutoff filter (KG-3, Schott) to reduce the mismatch in the region of 350–750 nm between the simulated light and AM 1.5 G to less than 4%.

SEM characterization

Cross-sectional scanning electron microscopy (SEM) and energy dispersive X-ray spectroscopy (EDX) were carried out using a MERLIN high-resolution SEM (Zeiss, Germany). The sample for SEM measurement was made by removing the PEDOT counter electrode of the solid-state DSSCs.

Incident photon-to-current conversion efficiency (IPCE)

IPCE spectra were measured with a lock-in amplifier (Stanford Research SystemSR830 DSP) under chopped monochromatic light (2 Hz) generated by a white light source from a 300 W xenon lamp passing through a Gemini-180 double monochromator (Jobin Yvon Ltd). The solar cell is illuminated under a constant white light bias with an intensity of 50 W m^{-2} supplied by an array of white light-emitting diodes.

Transient photocurrent and photovoltage measurements

Electron lifetime measurements were performed using the DN-AE01 Dyenamo toolbox with a white LED (Luxeon Star 1W) as light source. Voltage traces were recorded with a 16-bit resolution digital acquisition board (National Instruments) and lifetimes were determined by monitoring photovoltage transients at different light intensities upon applying a small square wave modulation to the base light intensity. The photovoltage responses were fitted using first-order kinetics to obtain time constants.

Electrochemical impedance spectroscopy (EIS)

EIS measurements were performed with a BioLogic SP300 potentiostat. To obtain the spectra, the solar cell was biased with potentials and a modulation amplitude of 15 mV in the frequency range (1 MHz–0.1 Hz). Z-view software (Scribner) was used for analysis of the impedance spectra.

Flash photolysis measurement

The experiment was conducted with dye adsorbed on TiO_2 films in the presence of inert electrolytes (0.1 M LiTFSI and 0.5/0.6 M 4-*tert*-butylpyridine in acetonitrile for the cobalt/copper based electrolyte). To observe the microsecond-to-millisecond dynamics, a nanosecond laser pump pulse excites a sample and induces a photochemical reaction, while a continuous light source probes the response of the reaction. The excitation source is generated by a frequency-doubled (532 nm) Nd-YAG Q-switched laser (Ekspla NT-342) with 20 Hz repetition rate. To optimize the experimental fluence conditions, the pump beam is attenuated by grey filters. As the probe beam, a continuous Xenon arc lamp filtered by a monochromator with filters is used. The probe beam passing through a sample is collected by a second monochromator and delivered to a fast photomultiplier tube (R9910, Hamamatsu) supplied with 750 V, which converts photons into electrons. To obtain a satisfactory signal to noise ratio, a digital signal analyzer (DPO 7104C, Tektronix) records the induced transient voltage signal and the data acquisition is averaged over 3000 laser shots, resulting in a sensitivity of 10^{-4} ΔA.

Conflicts of interest

There are no conflicts of interest to declare.

Acknowledgements

The authors acknowledge financial support from NSFC for Creative Research Groups (21421004) and Key Project (21636002), NSFC/China, Oriental Scholarship, Fundamental Research Funds for the Central Universities (WJ1416005, WJ1714007). M. G., J.-E. M., H. W. B. acknowledges Swiss National Science Foundation (grant no. 200021-157135/1 and NCCR MUST research instrument) and CTI 17622.1 PFNM-NM, glass2energy SA (g2e), Villaz-St-Pierre, Switzerland. L. K. acknowledges support from the Czech Science Foundation (grant No. 13-07724S). W. W. Z. acknowledges the China Scholarship Council (CSC) for a PhD study fellowship.

Notes and references

1 B. O'Regan and M. Grätzel, *Nature*, 1991, **353**, 737–740.
2 A. Hagfeldt, G. Boschloo, L. Sun, L. Kloo and H. Pettersson, *Chem. Rev.*, 2010, **110**, 6595–6663.
3 D. Joly, L. Pelleja, S. Narbey, F. Oswald, T. Meyer, Y. Kervella, P. Maldivi, J. N. Clifford, E. Palomares and R. Demadrille, *Energy Environ. Sci.*, 2015, **8**, 2010–2018.
4 F. M. Jradi, X. Kang, D. O. Neil, G. Pajares, Y. A. Getmanenko, P. Szymanski, T. C. Parker, M. A. El-Sayed and S. R. Marder, *Chem. Mater.*, 2015, **27**, 2480–2487.
5 B. Xu, E. Sheibani, P. Liu, J. Zhang, H. Tian, N. Vlachopoulos, G. Boschloo, L. Kloo, A. Hagfeldt and L. Sun, *Adv. Mater.*, 2014, **26**, 6629–6634.
6 P. K. Nayak, J. Bisquert and D. Cahen, *Adv. Mater.*, 2011, **23**, 2870–2876.
7 H. J. Snaith, *Adv. Funct. Mater.*, 2010, **20**, 13–19.
8 B. E. Hardin, H. J. Snaith and M. D. McGehee, *Nat. Photonics*, 2012, **6**, 162–169.
9 S. Ardo and G. J. Meyer, *Chem. Soc. Rev.*, 2009, **38**, 115–164.
10 D. Zhou, Q. Yu, N. Cai, Y. Bai, Y. Wang and P. Wang, *Energy Environ. Sci.*, 2011, **4**, 2030–2034.
11 A. Yella, H. W. Lee, H. N. Tsao, C. Yi, A. K. Chandiran, M. K. Nazeeruddin, E. W. G. Diau, C. Y. Yeh, S. M. Zakeeruddin and M. Grätzel, *Science*, 2011, **334**, 629–634.
12 Z. Yao, M. Zhang, H. Wu, L. Yang, R. Li and P. Wang, *J. Am. Chem. Soc.*, 2015, **137**, 3799–3802.
13 S. Zhang, X. Yang, Y. Numata and L. Han, *Energy Environ. Sci.*, 2013, **6**, 1443–1464.
14 Y. Hao, W. Yang, L. Zhang, R. Jiang, E. Mijangos, Y. Saygili, L. Hammarström, A. Hagfeldt and G. Boschloo, *Nat. Commun.*, 2016, **7**, 13934.
15 N. Zhou, K. Prabakaran, B. Lee, S. H. Chang, B. Harutyunyan, P. Guo, M. R. Butler, A. Timalsina, M. J. Bedzyk, M. A. Ratner, S. Vegiraju, S. Yau, C. Wu, R. P. H. Chang, A. Facchetti, M. Chen and T. J. Marks, *J. Am. Chem. Soc.*, 2015, **137**, 4414–4423.
16 M. Freitag, Q. Daniel, M. Pazoki, K. Sveinbjornsson, J. Zhang, L. Sun, A. Hagfeldt and G. Boschloo, *Energy Environ. Sci.*, 2015, **8**, 2634–2637.
17 K. Kakiage, Y. Aoyama, T. Yano, K. Oya, J. Fujisawa and M. Hanaya, *Chem. Commun.*, 2015, **51**, 15894–15897.
18 C. Chou, F. Hu, H. Yeh, H. Wu, Y. Chi, J. N. Clifford, E. Palomares, S. Liu, P. Chou and G. Lee, *Angew. Chem., Int. Ed.*, 2014, **53**, 178–183.
19 M. Liang and J. Chen, *Chem. Soc. Rev.*, 2013, **42**, 3453–3488.
20 Z. Yao, M. Zhang, R. Li, L. Yang, Y. Qiao and P. Wang, *Angew. Chem., Int. Ed.*, 2015, **54**, 5994–5998.
21 C. Wang, J. Hu, C. Wu, H. Kuo, Y. Chang, Z. Lan, H. Wu, E. Wei-Guang Diau and C. Lin, *Energy Environ. Sci.*, 2014, **7**, 1392–1396.
22 H. Choi, C. Baik, S. O. Kang, J. Ko, M. Kang, M. K. Nazeeruddin and M. Grätzel, *Angew. Chem., Int. Ed.*, 2008, **47**, 327–330.
23 Z. Wang, N. Koumura, Y. Cui, M. Takahashi, H. Sekiguchi, A. Mori, T. Kubo, A. Furube and K. Hara, *Chem. Mater.*, 2008, **20**, 3993–4003.
24 Y. Xie, W. Wu, H. Zhu, J. Liu, W. Zhang, H. Tian and W. H. Zhu, *Chem. Sci.*, 2016, **7**, 544–549.
25 H. Li, T. M. Koh, A. Hagfeldt, M. Gratzel, S. G. Mhaisalkar and A. C. Grimsdale, *Chem. Commun.*, 2013, **49**, 2409–2411.
26 Y. Saygili, M. Söderberg, N. Pellet, F. Giordano, Y. Cao, A. B. Muñoz-García, S. M. Zakeeruddin, N. Vlachopoulos, M. Pavone, G. Boschloo, L. Kavan, J. Moser, M. Grätzel, A. Hagfeldt and M. Freitag, *J. Am. Chem. Soc.*, 2016, **138**, 15087–15096.
27 J. Cong, D. Kinschel, Q. Daniel, M. Safdari, E. Gabrielsson, H. Chen, P. H. Svensson, L. Sun and L. Kloo, *J. Mater. Chem. A*, 2016, **4**, 14550–14554.
28 J. Yum, E. Baranoff, F. Kessler, T. Moehl, S. Ahmad, T. Bessho, A. Marchioro, E. Ghadiri, J. Moser, C. Yi, M. K. Nazeeruddin and M. Grätzel, *Nat. Commun.*, 2012, **3**, 631.
29 M. Freitag, J. Teuscher, Y. Saygili, X. Zhang, F. Giordano, P. Liska, J. Hua, S. M. Zakeeruddin, J. Moser, M. Grätzel and A. Hagfeldt, *Nat. Photonics*, 2017, **11**, 372–378.
30 Y. Cao, Y. Saygili, A. Ummadisingu, J. Teuscher, J. Luo, N. Pellet, F. Giordano, S. M. Zakeeruddin, J. E. Moser, M. Freitag, A. Hagfeldt and M. Grätzel, *Nat. Commun.*, 2017, **8**, 15390.
31 M. Freitag, F. Giordano, W. Yang, M. Pazoki, Y. Hao, B. Zietz, M. Grätzel, A. Hagfeldt and G. Boschloo, *J. Phys. Chem. C*, 2016, **120**, 9595–9603.
32 S. Kim, J. K. Lee, S. O. Kang, J. Ko, J. H. Yum, S. Fantacci, F. De Angelis, D. Di Censo, M. K. Nazeeruddin and M. Grätzel, *J. Am. Chem. Soc.*, 2006, **128**, 16701–16707.
33 D. Kuang, S. Uchida, R. Humphry-Baker, S. M. Zakeeruddin and M. Grätzel, *Angew. Chem., Int. Ed.*, 2008, **47**, 1923–1927.
34 H. N. Tsao, C. Yi, T. Moehl, J. Yum, S. M. Zakeeruddin, M. K. Nazeeruddin and M. Grätzel, *ChemSusChem*, 2011, **4**, 591–594.
35 W. H. Zhu, Y. Wu, S. Wang, W. Li, X. Li, J. Chen, Z. Wang and H. Tian, *Adv. Funct. Mater.*, 2011, **21**, 756–763.
36 Y. Wu and W. H. Zhu, *Chem. Soc. Rev.*, 2013, **42**, 2039–2058.
37 A. Yella, R. Humphry-Baker, B. F. E. Curchod, N. Ashari Astani, J. Teuscher, L. E. Polander, S. Mathew, J. Moser, I. Tavernelli, U. Rothlisberger, M. Grätzel, M. K. Nazeeruddin and J. Frey, *Chem. Mater.*, 2013, **25**, 2733–2739.

38 W. S. Yang, B. Park, E. H. Jung, N. J. Jeon, Y. C. Kim, D. U. Lee, S. S. Shin, J. Seo, E. K. Kim, J. H. Noh and S. I. Seok, *Science*, 2017, **356**, 1376.
39 C. Teng, X. Yang, C. Yuan, C. Li, R. Chen, H. Tian, S. Li, A. Hagfeldt and L. Sun, *Org. Lett.*, 2009, **11**, 5542–5545.
40 F. Fabregat-Santiago, G. Garcia-Belmonte, I. Mora-Sero and J. Bisquert, *Phys. Chem. Chem. Phys.*, 2011, **13**, 9083–9118.
41 K. Pei, Y. Wu, A. Islam, Q. Zhang, L. Han, H. Tian and W. H. Zhu, *ACS Appl. Mater. Interfaces*, 2013, **5**, 4986–4995.
42 X. Zhang, Y. Xu, F. Giordano, M. Schreier, N. Pellet, Y. Hu, C. Yi, N. Robertson, J. Hua, S. M. Zakeeruddin, H. Tian and M. Grätzel, *J. Am. Chem. Soc.*, 2016, **138**, 10742–10745.
43 K. Pei, Y. Wu, W. Wu, Q. Zhang, B. Chen, H. Tian and W. H. Zhu, *Chem. – Eur. J.*, 2012, **18**, 8190–8200.